Appl. Phys. A 89, 685–693 (2007)
DOI: 10.1007/s00339-007-4149-8

Applied Physics A
Materials Science & Processing

Y. ZHANG[1,✉]
X. CHENG[1,2]
S. ZHANG[3]

In-situ Raman spectroscopic study of domain switching of PLZT ceramics

[1] Department of Materials Science and Engineering, Xiamen University, Xiamen, FJ 361005, P.R. China
[2] State Key Laboratory for Physical Chemistry of Solid Surfaces, Xiamen University, Xiamen, FJ 361005, P.R. China
[3] Department of Chemistry, Xiamen University, Xiamen, FJ 361005, P.R. China

Received: 12 October 2006/Accepted: 22 May 2007
Published online: 27 June 2007 •

ABSTRACT A specially designed apparatus was used to observe in-situ domain switching in lanthanum-doped lead zirconate titanate (PLZT) ceramics by Raman spectroscopy. Using the established technique, the variations in measured Raman spectrum of unpoled and appropriately poled PLZT ceramics under the application of dc voltage and during the process of electric fatigue were examined. It was confirmed that the intensity change in the soft mode of the Raman band is highly dependent on the orientation of the domain switching with respect to the polarization direction of Raman incident light. When the orientation of the specimen with respect to propagation directions (including polarization direction) of incident light and scattered light is appropriate, the Raman spectroscopy can allow a non-destructive and in-situ measurement of the domain switching in a microscopic scale. The relation between the domain switching and the measured Raman spectrum change is discussed for PLZT polycrystalline materials by developing criteria extended from a single-crystal model.

PACS 81.70.Fy; 78.30.-j; 62.20.Mk

1 Introduction

Domain switching, fatigue behavior caused by a change in spontaneous polarization direction due to an electrical or/and a mechanical cyclic load, has been considered to be a major cause that leads to deterioration in properties of ferroelectric ceramics such as barium titanate, lead zirconate and lead zirconate titanate (PZT) or lanthanum-doped PZT (PLZT) [1–7]. Several ferroelectric fatigue mechanisms have been suggested which scale in size from point defects to macroscopic boundary conditions [8]. Due to a critical lack of in-situ and non-destructive methods, the microscopic fatigue mechanism for ferroelectric materials has not been well understood yet. Much effort has been devoted to develop applicable techniques or to establish reliable methods through which direct evidence of domain switching in ferroelectric ceramics under electrical and/or mechanical loads can be provided. Microscopic techniques such as scanning force microscopy (SFM) [9–11], scanning electron microscopy (SEM) [12, 13] and transmission electron microscopy (TEM) [13–15] could accomplish a direct observation of domain switching at a nanoscale or microscale; particularly, a random domain switching generated by an alternating electric field in $BaTiO_3$ single crystal [11], as well as nanodomain alignment, grain boundary cracking and domain boundary cracking induced by a cyclic electric field in fine- or coarse-grained ceramics and single crystals [14] were observed through in-situ atomic force microscopy (AFM) and TEM investigations. On the other hand, in-situ X-ray diffraction (XRD) measurements could perform a quantitative analysis based on the relative peak intensity of tetragonal (002) and (200) for the domain switching of PZT [16, 17] or PLZT [18–20] under an applied electric field, with the electric-field-induced domain switching of PLZT and its relation to the ferroelectric properties during an electric fatigue being further probed [19, 20]. The direct observations of the domain switching in the ferroelectric materials have greatly enhanced the fundamental understanding of degradation and the failure micromechanism. However, the aforementioned in-situ methods have severe disadvantages and limitations. For example, an X-ray beam normally would cover many crystal grains in materials under study; thus, an in-situ XRD measurement can only provide a sort of statistical information in a domain over a macroscale. On the other hand, a specimen used for SEM or TEM observation must be prepared by chemical etching or by cutting and being thinned down to be electron transparent; therefore, this must be destructive. The data that in-situ SEM or TEM observation gives cannot directly be correlated to bulk materials in real service. Moreover, specimens used for SEM and TEM observations must be placed in a high-vacuum chamber; hence, the investigations are costly and inconvenient.

Raman spectroscopy is a promising and effective tool to study ferroelectric phase transformations and ferroelectric properties at various temperatures or pressures [21–30]. A laser beam used for Raman incident light can generate a very small spot (typically of $\sim 3\ \mu m$) and is thus suitable for the detection of scattered light by a highly localized area of the microscale. Hence, it is feasible to obtain the light signals scattered by a single grain of micrometer scales ($> 3\ \mu m$) by focusing the laser beam on the surface of the grain. In addition, Raman spectroscopy does not require a high-vacuum chamber or an electron-transparent specimen for operation as does SEM or TEM. Therefore, Raman spectroscopic analysis for ferroelectric domain switching can be in-situ realized

✉ Fax: +86-592-218-3937, E-mail: yzh@xmu.edu.cn

under the applications of external fields with such flexibility. Previous studies using Raman spectroscopy have been mostly carried out for crystal structure of ferroelectric materials such as lattice and soft modes, phase transformation or evolution, domain orientation, mainly for lead titanate (PT) single crystals or polycrystalline powders [22–29], while the phonon dynamics of PLZT-x/95/5 ($1 \leq x \leq 4$ mol. %) [30], the residual stresses in PZT thin films [31] and the phase transition in screen-printed PZT thick films [32] have also been investigated with Raman spectroscopy. However, little information is available for in-situ Raman observations on domain switching in ferroelectric ceramics under an electrical load.

Our earlier work [33] indicated that the domain switching in PLZT ceramics could be in-situ observed by Raman spectroscopy. This investigation was extended to develop a better-controlled non-destructive method by fabricating a special experimental apparatus to be associated with a Raman spectrometer for in-situ observation of domain switching and, more importantly, to explain the cause of the Raman spectrum change due to domain switching in PLZT ceramics. The Raman spectra before and after 90° rotation of an unpoled or an appropriately poled PLZT ceramic were in-situ measured under the application of dc voltage or during the process of electric fatigue. The relation between the domain switching and the measured changes in the Raman spectrum, as well as the ferroelectric properties of PLZT before and after the electric fatigue, is examined.

2 Experimental

2.1 *Materials and electrode preparation*

The PLZT samples were purchased from the Institute of Acoustics, Chinese Academy of Sciences. The atomic ratio of samples for Zr/Ti was 53/47 with an additional doping of 3% atomic ratio of La and Nb. The specimens were in a rectangular shape with a dimension of $0.8 \times 8 \times 8\,\mathrm{mm}^3$, and some were polarized along either the transverse or perpendicular direction during the preparation of the materials. In this article, the in-plane and out-of-plane poled specimens refer to the specimens that were arranged in the experiments so that their polarization directions were parallel to the Z-axis (cf. Fig. 1b) or to the X-axis (the normal to the $8 \times 8\,\mathrm{mm}^2$ surface), respectively.

In order to ensure the applied electrical field (E_A) being larger than the coercive electrical field (E_C) of the materials and safety in the application of high voltages during the Raman spectroscopic measurement, the specimens were intentionally etched for a groove 0.2-mm wide in the middle of the $8 \times 8\,\mathrm{mm}^2$ surface by lithography after a thin layer of silver was deposited on the surface. The silver layer within the groove was then removed, whereas the silver layer on both sides of the groove remained, which served as two electrodes for the subsequent electrical load. The grooves at the electrodes must be entirely parallel and flat, thus ensuring a uniform voltage to be applied between the two electrodes after an electrical field is applied. When a voltage of 200 V is applied to the specimens, a strength of 1000 V/mm, which is about the value of the coercive electric field of the specimens, will be produced in the ceramics between the two electrodes, without infringing the safety of the apparatus.

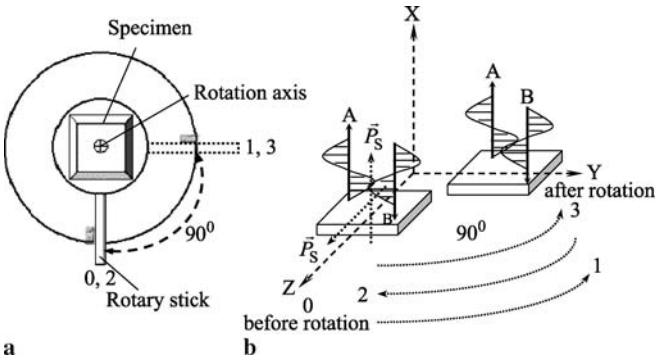

FIGURE 1 Schematic representations for in-situ Raman spectroscopic measurements. (**a**) 90° rotation apparatus; (**b**) orientation of specimens with respect to polarization directions of incident and scattered light. $\boldsymbol{P}_\mathrm{S}$ – orientation of the specimens ($\boldsymbol{P}_\mathrm{S} /\!/ Z$-axis: in-plane poled; $\boldsymbol{P}_\mathrm{S} /\!/ X$-axis: out-of-plane poled); A – polarized backscattered light; B – polarized incident light

2.2 *Apparatus and Raman measurements*

The Raman spectra were collected on a Raman micro spectroscope (Jobin Yvon LabRam I) with confocal microscope (Dilor Inc., France). The excitation source was a 4 mW polarized He–Ne laser with a wavelength of 632 nm. The lens for collecting scattered light was an objective lens with 50 times magnification. The time of exposure was 10 s. During each measurement, an optical microscope was used to locate the site illuminated by the laser so as to ensure that the spot of the laser beam is at the central portion of each grain to reduce the effect of grain boundaries.

To observe in-situ domain switching in the specimens, a special apparatus was designed and fabricated to enable a 90° rotation of the specimens during Raman spectroscopic measurement and is schematically illustrated in Fig. 1. As can be seen in Fig. 1a, the specimen was held in the center of the apparatus, and could be rotated 90° either clockwise or counterclockwise with a rotary stick. After a 90° rotation of a specimen about the X-axis (counterclockwise rotation), an originally in-plane poled specimen will be rotated by 90° so that its polarization direction is parallel to the Y-axis as shown in Fig. 1b. With respect to the scattered light and the incident light (A and B in Fig. 1b) polarized in the direction parallel to the Y-axis, the counterclockwise 90° rotation of an in-plane poled specimen was equivalent to the occurrence of a 90° domain switching in the specimen. On the other hand, with the same rotation, the polarization direction of an originally out-of-plane poled specimen will remain unchanged (parallel to the X-axis) with respect to the aforementioned scattered and incident light. Consequently, we would not expect such a rotation producing domain switching with respect to the laser beam.

Raman spectroscopic measurements were carried out using the established technique under the application of an electric field or during the process of electric fatigue. A series of dc voltages were applied to unpoled, in-plane or out-of-plane poled PLZT specimens for 5 min according to the following sequence: 0 V → 80 V → 120 V → 160 V → 200 V → 240 V → 280 V → 320 V → 360 V → 400 V. As illustrated in Fig. 1, the direction of the applied electric field (E_A) was along the Z-axis, the polarization direction of the

laser beam was parallel to the Y-axis, while the polarization directions of in-plane and out-of-plane poled specimens were along the Z-axis and X-axis, respectively. During processes of electric fatigue, the three types of PLZT specimens were subjected to an electric fatigue by various cycles (N) from $0 \rightarrow 10^4 \rightarrow 10^5 \rightarrow 10^{5.8} \rightarrow 10^6 \rightarrow 10^{6.2} \rightarrow 10^7$. Raman spectra were collected immediately after each voltage application or each electric fatigue cycle. The hysteresis loops were also measured before and after each fatigue cycle using a RT6000HVS measuring system (Radiant Technology, USA).

3 Results

3.1 *In-situ Raman observation of 90° domain switching*

Figure 2 presents the surface morphologies of as-received unpoled, out-of-plane and in-plane poled PLZT samples. The grain sizes of the three types of PLZT samples were 1–3 μm as evident in Fig. 2. The as-received PLZT samples were in tetragonal phase with lattice parameters of $a = b = 0.4047$ nm and $c = 0.4120$ nm, determined by XRD using a Rigaku D/Max-RC X-ray diffractometer (Japan). The average E_C values were evaluated to be 1135, 995 and 930 V/mm for the unpoled, out-of-plane and in-plane poled PLZT ceramics, respectively, based on their characteristic hysteresis loops.

Typical Raman spectra of the unpoled PLZT ($PbZr_{0.53}Ti_{0.47}O_3$) polycrystalline samples are compared with that of PT ($PbTiO_3$) single crystal [23] in Fig. 3. The corresponding Raman soft modes for tetragonal perovskite PT single crystals are labeled in the figure based on the previous studies [22–24]. It is apparent that the Raman bands observed from the PT single crystal were sharper and well defined for each soft mode. The broadening of Raman bands in the PLZT samples was observed and this caused overlapping in Raman soft modes as compared with PT in Fig. 3. In the range of 100–400 cm^{-1}, three well-defined soft modes in PT, E(2TO), $E(3TO + 2LO) + B_1$ and $A_1(2TO)$, formed a broad Raman band in PLZT, which might be attributed to the change of crystalline structure due to variations in the chemical compositions as well as the effects of the polycrystalline structures of the material on the Raman bands. In addition, temperature and pressure may also strongly influence the shape and position of Raman spectra caused by phase transformation in ferroelectric materials [25–29].

More accurate identification in Raman bands observed for PLZT samples as shown in Fig. 3 requires further detailed study and is beyond the scope of this investigation. The main focus of this work was to establish an in-situ Raman observation method and to relate the measured intensity change in Raman bands with domain switching in the PLZT samples. For the sake of analysis, only the Raman bands observed in the range of 100–400 cm^{-1} are discussed in this article although a full range of Raman spectra was measured. Two Raman bands appearing in the range of 100–400 cm^{-1} in Fig. 3 can be roughly assigned to O–(Zr,Ti)–O bending vibration at ~ 212 cm^{-1} (E(2TO) mode) and $(Zr,Ti)O_3$ torsion at ~ 280 cm^{-1} ($E(3TO + 2LO) + B_1$ mode) based on the previous studies [25–29].

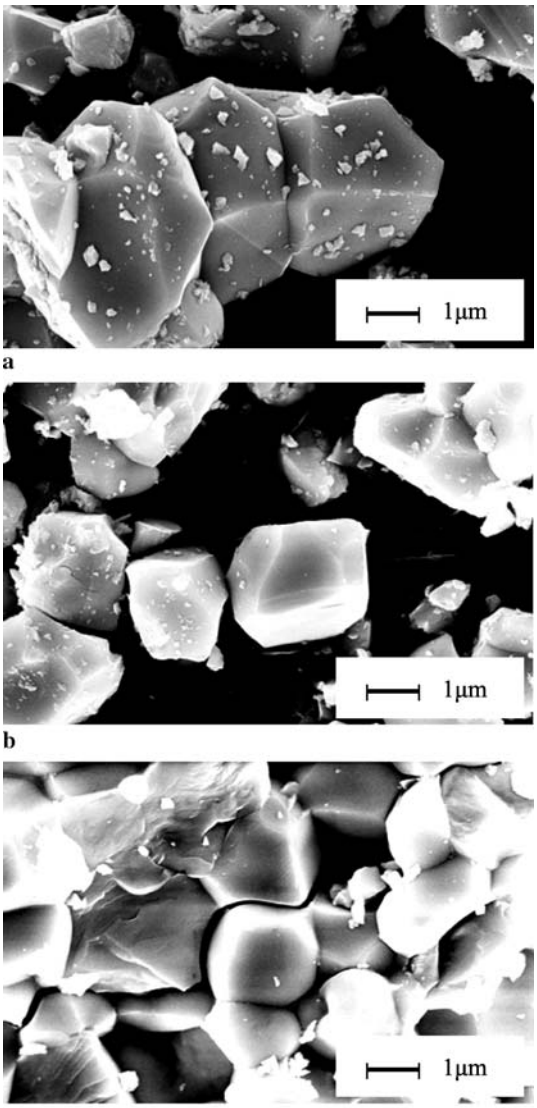

FIGURE 2 Surface morphologies of PLZT ceramics; (**a**) unpoled; (**b**) out-of-plane poled; (**c**) in-plane poled

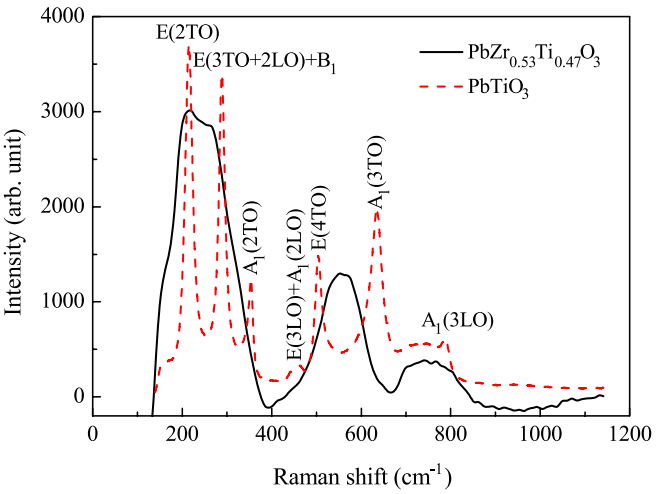

FIGURE 3 Typical Raman spectra obtained from unpoled PLZT polycrystalline ceramics and $PbTiO_3$ single crystal

The Raman spectra obtained before and after a 90° in-situ rotation for the three types of PLZT specimens are presented in Fig. 4. It is obvious from Fig. 4a that the intensities of both Raman bands corresponding to E(2TO) and E(3TO + 2LO) + B_1 soft modes remained virtually unchanged for both unpoled and originally out-of-plane poled specimens. However, we observed an appreciable change in the intensities of the spectra for the in-plane poled specimens. In Fig. 4b, the labels 0–3 indicate the spectra of an in-plane poled specimen at consecutive positions after each 90° rotation. Label 0 corresponds to the initial position of the specimen (i.e. the polarization direction is parallel to the Z-axis), 1 to the position after a 90° counterclockwise rotation from position 0, 2 to the position after a 90° clockwise rotation from position 1 and 3 to the position after a 90° counterclockwise rotation from position 2. From Fig. 4b, it is clear that the intensity of the spectrum increased substantially when the specimen was rotated from position 0 to position 1, then dropped back to the original level after the specimen was rotated from position 1 to position 2, and rose to the level associated with position 1 after the specimen was rotated again from position 2 to position 3.

Statistically speaking, an unpoled specimen has no preferred polarization orientations; therefore, it is reasonable to expect that any rotations of the specimen will cause no change of the polarization direction of the specimen. For an out-of-plane poled specimen, the favorite orientation of polarization is along the X-axis and, in the plane defined by the X-axis, there are no favorite orientation projections of polarization statistically. Consequently, any rotations of such specimens about the X-axis will result in no changes in the in-plane projections of polarization orientation. For an in-plane poled specimen, the 90° rotation of the specimen about the X-axis implies a 90° change in the polarization orientation. Clearly, from the above experimental observations, there are virtually no changes in the intensities of Raman spectra for the unpoled and the out-of-plane poled specimens, and there is a substantial change in the intensities of Raman spectra for the in-plane poled specimen. The above analysis seems to indicate that the variations in the Raman intensities observed from the 90° back-and-forth rotation measurements may be directly attributed to the 90° change of the polarization orientation of specimens with respect to the polarized incident and scattered light. Since the polarization direction of the incident and scattered light is along the Y-axis, Fig. 4b also indicates that when the polarization orientation of the specimen is parallel to the polarization directions of the incident and scattered light, the Raman intensity becomes stronger compared with that associated with the specimen having a polarization orientation perpendicular to the polarization directions of the incident and scattered light (the Y-axis in this case).

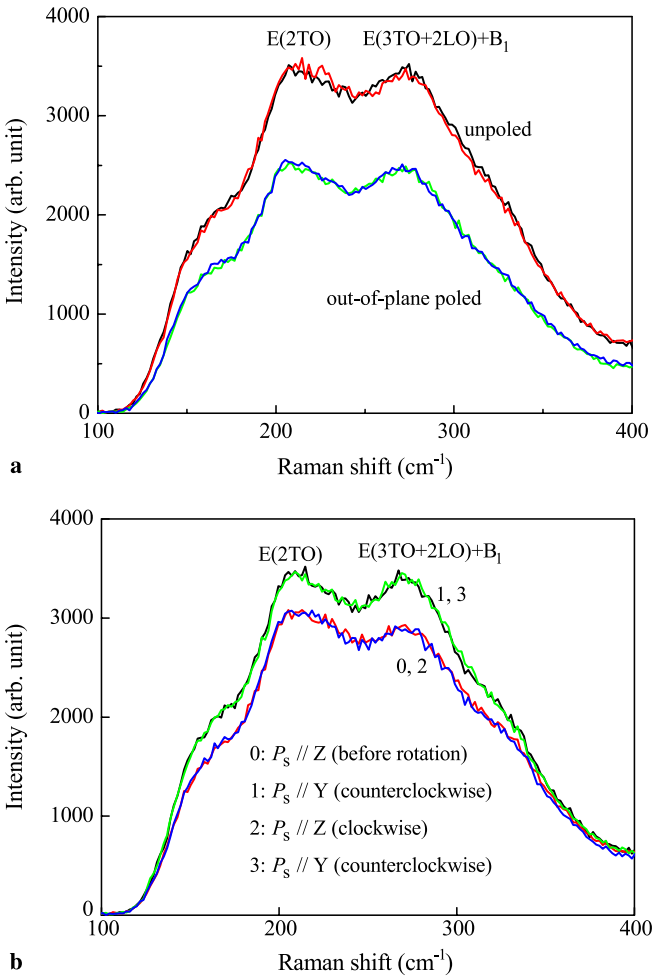

FIGURE 4 In-situ Raman spectra measured before and after different 90° rotations illustrated in Fig. 1; (**a**) unpoled and out-of-plane poled; (**b**) in-plane poled

3.2 *90° domain switching under an applied electric field*

Figure 5 compares the in-situ Raman spectra for the unpoled, out-of-plane and in-plane poled PLZT specimens, obtained under the application of dc voltage, as indicated in Fig. 1b; the direction of E_A is along the Z-axis (Fig. 5a–c) and during the process of an electric fatigue (Fig. 5a′–c′). The direction of arrows in the figure indicates the increase of electric field strength or fatigue cycle number. It is apparent that the intensities of the measured Raman spectra declined notably with the increases in the magnitude of the electric field and the cycle number of the electric fatigue. More quantitative information of the intensity changes of Raman bands measured under the application of an electric field or during the electric fatigue is presented in Fig. 6 by plotting the relative intensities against the relative strength of the electric field or the cycle number during electric fatigue. Here, the relative intensities are defined as a ratio between the Raman intensity at an applied electric field (I^E) or during a cycle of the electric fatigue (I^N) and the Raman intensity before application of electric field or fatigue (I^0). It is interesting to note that the out-of-plane poled PLZT specimens exhibited the most significant reduction in the relative intensity when the magnitude of the applied electric field (E_A) or the cycle number (N) of the electric fatigue increased. A rapid decline ($\sim 30\%$) in the relative Raman intensities was observed at $E_A \leq 0.6E_C$ with a much slower decrease after further increase of E_A, particularly when $E_A \geq 1.2E_C$ as can be seen in Fig. 6a. In the case of an electric fatigue process, as evident in Fig. 6b, a rapid decrease occurred for all the three specimens near $N = 10^{6.2}$, which accounts for more than a 20% reduction, and then decreased appreciably afterwards.

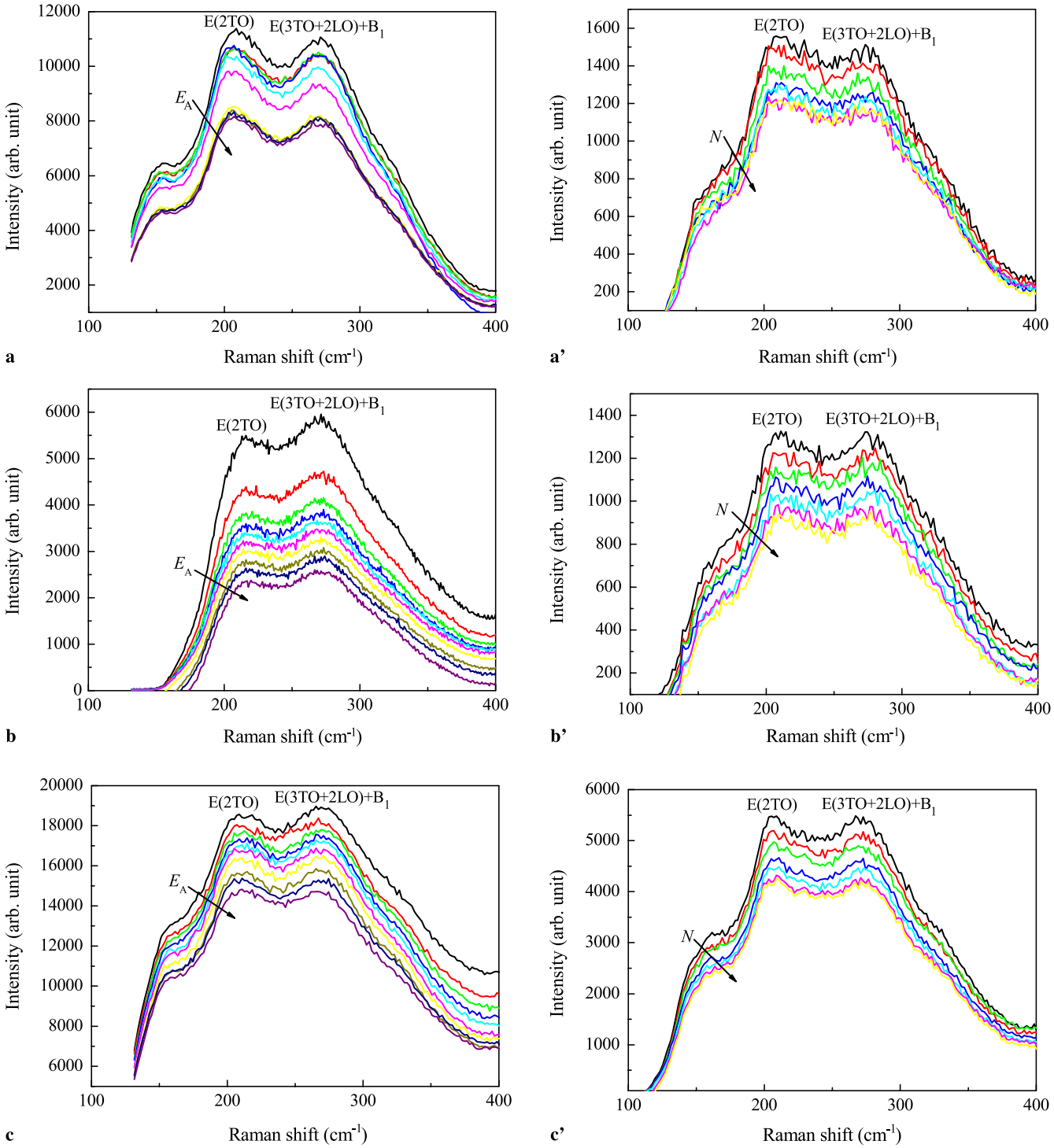

FIGURE 5 In-situ Raman spectra of PLZT specimens under the application of various electrical fields (*left*) or during different cycles of electric fatigue (*right*). *Arrows* indicate the increase in electric field strength or electric fatigue cycle number; (**a**, **a**′) unpoled; (**b**, **b**′) out-of-plane poled; (**c**, **c**′) in-plane poled

The variations in the relative change in polarization intensity of specimens, i.e. a ratio of remanent polarization intensity during and before the electric fatigue (P_r^N/P_r^0), with cycle number are also included in Fig. 6b. From Fig. 6b, it is clear that the ratio P_r^N/P_r^0 for the out-of-plane poled PLZT specimen appeared to decrease more quickly as the number of cycles increases than those of unpoled and in-plane poled PLZT specimens do. We further notice from Fig. 6b that the variation curves of P_r^N/P_r^0 for the three types of specimens all showed a clear turning point at $N = 10^{6.2}$ that is consistent with the variation curves for relative Raman intensity.

4 Discussion

Raman spectroscopy is a powerful tool for the study of ferroelectric materials at a microscopic scale. However, understandings associated with the intensity of the scattering spectra are quite complex both theoretically and ex-

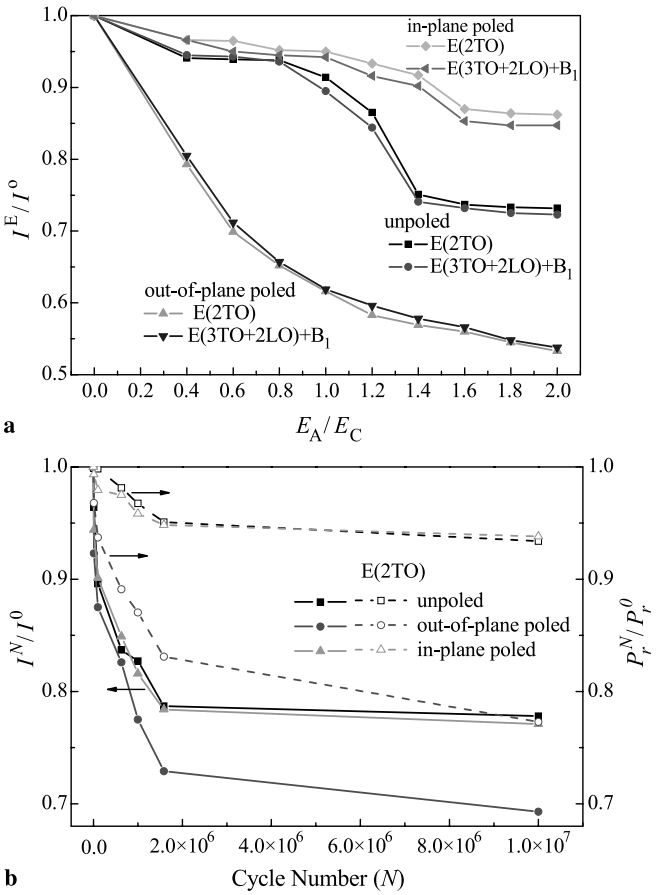

FIGURE 6 Variations in the relative intensities of Raman soft modes with the electric field strength and cycle number of electric fatigue as well as remanent polarization; (**a**) I^E/I^0 vs. E_A/E_C; (**b**) I^N/I^0 vs. N and P_r^N/P_r^0

perimentally. The interpretations of Raman spectra in relation to phase transformation, ferroelectric property, temperature and angular effects have been presented for PT single crystals or polycrystalline powders [25–29]. A complete quantitative analysis for the relation between the intensity of the Raman spectrum and the domain switching in ferroelectrics at the microscopic level requires insight into the scattering mechanism and microstructure available for the polycrystalline PLZT ceramics. In the following section, an attempt was made to explain how the measured Raman intensity change could be related to the electrically induced 90° domain switching in PLZT ceramics by developing criteria extended from the PT single crystal model.

When treated by a macroscopic theory, the induced dipole moments of the individual atoms are normally added together as a macroscopic polarization vector in a continuum medium. Considering that the displacement of the crystal lattice vibration is very small under excitation of the incident light, the intensity I_S of Raman scattered light for a single crystal may be written as

$$I_S = 2\varepsilon_0 n_S c|\boldsymbol{E}_S|^2 , \tag{1}$$

where ε_0 is the dielectric constant in vacuum, n_S the refractive index of scattered light, c the speed of light and $\boldsymbol{E}_S$ the electric field associated with the induced polarization.

The polarization $\boldsymbol{P}_S$ induced by incident light may be approximately expressed as

$$\boldsymbol{P}_S \approx \varepsilon_0 \left[\underline{\underline{\chi}}(0) + \left. \frac{\partial \underline{\underline{\chi}}(\boldsymbol{u})}{\partial \boldsymbol{u}} \right|_{\boldsymbol{u}=0} \boldsymbol{u} \right] \boldsymbol{E}_I , \tag{2}$$

where $\underline{\underline{\chi}}(0)$ represents the induced polarizability tensor when crystal lattices are in their equilibrium positions, which is related to elastic scattering of the beam; whereas $\partial \underline{\underline{\chi}}(\boldsymbol{u})/\partial \boldsymbol{u}\big|_{\boldsymbol{u}=0}$ is the derivative of the second-rank polarizability tensor or polarizability, which is a third-rank tensor and is related to inelastic scattering of the beam, namely, it is related to Raman scattering, $\boldsymbol{u}$ is the displacement of crystal lattice vibration and $\boldsymbol{E}_I$ is the electric field of the incident light. Equation (2) indicates that $\boldsymbol{P}_S$ is related to $\underline{\underline{\chi}}(\boldsymbol{u})$. Because domain switching in the scattering body may directly lead to a change in $\underline{\underline{\chi}}(\boldsymbol{u})$, a variation in the intensity of $\boldsymbol{P}_S$ and the intensity of Raman scattered light I_S is expected through altering $\underline{\underline{\chi}}(\boldsymbol{u})$.

As mentioned earlier, the Raman band appearing at $\sim 212\,\mathrm{cm}^{-1}$ can be roughly assigned to O–(Zr,Ti)–O bending vibration corresponding to soft mode E(2TO). Figure 7 schematically depicts the possible bending vibration modes for the O–(Zr,Ti)–O plane in tetragonal phase of PLZT single crystal. Provided that the Z direction in Fig. 7 is the direction for the spontaneous polarization in the material (or electric domain orientation), the PLZT in tetragonal phase will have three basic modes for O–(Zr,Ti)–O bending vibrations, namely, bending vibrations along $\boldsymbol{a}$, $\boldsymbol{b}$ and $\boldsymbol{c}$, respectively. Equation (2) can be further expressed in terms of the induced polarization of the elastic scattering $\boldsymbol{P}_S^e$ and the induced polarization of the inelastic scattering $\boldsymbol{P}_S^R$ as

$$\boldsymbol{P}_S \approx \varepsilon_0 \left[\underline{\underline{\chi}}(0) + \frac{\partial \underline{\underline{\chi}}(0)}{\partial \boldsymbol{u}} \boldsymbol{u} \right] \boldsymbol{E}_I = \boldsymbol{P}_S^e + \boldsymbol{P}_S^R , \tag{3}$$

$$\boldsymbol{P}_S^e = \varepsilon_0 \underline{\underline{\chi}}(0) \boldsymbol{E}_I , \tag{3a}$$

$$\boldsymbol{P}_S^R = \varepsilon_0 \left[\frac{\partial \underline{\underline{\chi}}(0)}{\partial \boldsymbol{u}} \boldsymbol{u} \right] \boldsymbol{E}_I , \tag{3b}$$

where $\partial \underline{\underline{\chi}}(0)/\partial \boldsymbol{u} = \partial \underline{\underline{\chi}}(\boldsymbol{u})/\partial \boldsymbol{u}\big|_{\boldsymbol{u}=0}$.

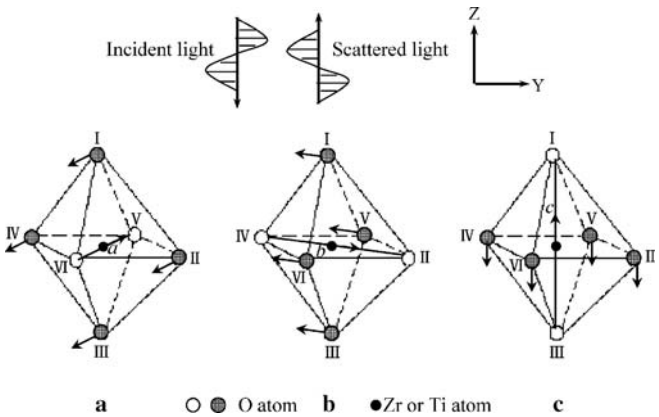

FIGURE 7 A schematic illustration of O–(Zr,Ti)–O plane bending vibration mode for tetragonal phase of PLZT single crystal; (**a**) along *a*-axis; (**b**) along *b*-axis; (**c**) along *c*-axis

If

$$\boldsymbol{E}_{\mathrm{I}} = \{E_a, E_b, E_c\}\,, \quad \boldsymbol{u} = \{u_a, u_b, u_c\} \tag{4}$$

then

$$\frac{\partial \underline{\underline{\chi}}(0)}{\partial \boldsymbol{u}}\boldsymbol{u} = \begin{Bmatrix} \chi_{11,a}u_a + \chi_{11,b}u_b + \chi_{11,c}u_c & \chi_{12,a}u_a + \chi_{12,b}u_b + \chi_{12,c}u_c & \chi_{13,a}u_a + \chi_{13,b}u_b + \chi_{13,c}u_c \\ \chi_{21,a}u_a + \chi_{21,b}u_b + \chi_{21,c}u_c & \chi_{22,a}u_a + \chi_{22,b}u_b + \chi_{22,c}u_c & \chi_{23,a}u_a + \chi_{23,b}u_b + \chi_{23,c}u_c \\ \chi_{31,a}u_a + \chi_{31,b}u_b + \chi_{31,c}u_c & \chi_{32,a}u_a + \chi_{32,b}u_b + \chi_{32,c}u_c & \chi_{33,a}u_a + \chi_{33,b}u_b + \chi_{33,c}u_c \end{Bmatrix}. \tag{5}$$

For a tetragonal state material with $P4mm$ crystal lattice, the three directions $\boldsymbol{a}$, $\boldsymbol{b}$ and $\boldsymbol{c}$ may be used to denote the three edges of the tetragonal lattice, which must fulfill the following relation:

$$\boldsymbol{a} \perp \boldsymbol{b} \perp \boldsymbol{c}\,. \tag{6}$$

Obviously, in tetragonal lattices two of the three edges have the same length. Employing three unit vectors along the three directions as the base vectors, and denoting them as 1, 2 and 3, respectively, the induced polarization $\boldsymbol{P}_{\mathrm{S}}^{\mathrm{R}}$ of the inelastic scattering along $\boldsymbol{a}$, $\boldsymbol{b}$ and $\boldsymbol{c}$ may be written as

$$\begin{aligned} \boldsymbol{E}_{\mathrm{I}}^{(100)} &= (1,0,0)E\,, \\ \boldsymbol{P}_{\mathrm{S}}^{\mathrm{R}}(100) &= \begin{Bmatrix} \chi_{11,a}u_a + \chi_{11,b}u_b + \chi_{11,c}u_c \\ \chi_{21,a}u_a + \chi_{21,b}u_b + \chi_{21,c}u_c \\ \chi_{31,a}u_a + \chi_{31,b}u_b + \chi_{31,c}u_c \end{Bmatrix} E\,, \\ \boldsymbol{E}_{\mathrm{I}}^{(010)} &= (0,1,0)E\,, \\ \boldsymbol{P}_{\mathrm{S}}^{\mathrm{R}}(010) &= \begin{Bmatrix} \chi_{12,a}u_a + \chi_{12,b}u_b + \chi_{12,c}u_c \\ \chi_{22,a}u_a + \chi_{22,b}u_b + \chi_{22,c}u_c \\ \chi_{32,a}u_a + \chi_{32,b}u_b + \chi_{32,c}u_c \end{Bmatrix} E\,, \\ \boldsymbol{E}_{\mathrm{I}}^{(001)} &= (0,0,1)E\,, \\ \boldsymbol{P}_{\mathrm{S}}^{\mathrm{R}}(001) &= \begin{Bmatrix} \chi_{13,a}u_a + \chi_{13,b}u_b + \chi_{13,c}u_c \\ \chi_{23,a}u_a + \chi_{23,b}u_b + \chi_{23,c}u_c \\ \chi_{33,a}u_a + \chi_{33,b}u_b + \chi_{33,c}u_c \end{Bmatrix} E\,. \end{aligned} \tag{7}$$

Here, the first pair of the expressions in (7) is for the case that the polarized incident light has a strength E and a vibration direction along the lattice direction $\boldsymbol{a}$; the second and third pairs in (7) are for the cases that the polarized incident light has the same strength as the first case but the vibration directions are along the lattice directions $\boldsymbol{b}$ and $\boldsymbol{c}$, respectively. Owing to the differences in the axis length, the expressions for the coefficients $\chi_{ij,k}$ ($i, j = 1, 2, 3$, $k = a, b, c$) appearing in (7) are, in general, different. Therefore, the values of $\boldsymbol{P}_{\mathrm{S}}^{\mathrm{R}}$ along $\boldsymbol{a}$, $\boldsymbol{b}$ and $\boldsymbol{c}$ directions of the vibration modes would be expected to be different accordingly.

Clearly, (7) provides us with the way to evaluate the induced polarization $\boldsymbol{P}_{\mathrm{S}}^{\mathrm{R}}$ for the cases when the incident light vibrates along three perpendicular lattice directions. For the sake of interpreting the experimental phenomenon, let us consider the case where the polarization direction of the incident light is fixed. Suppose that the polarized incident light travels along the X direction and vibrates in the Y direction as shown in Fig. 1b. Suppose also that a tetragonal ferroelectric lattice lies in a way such that its direction of polarization (for example, the direction along edge $\boldsymbol{c}$ of the lattice) is along the Z direction and one of the other two edges is along the X direction (say, edge $\boldsymbol{a}$). When the tetragonal lattice of the ferroelectric crystal is rotated 90° about the X-axis, it would be equivalent to the situation where the lattice is fixed in space and the polarization direction of the incident light is rotated from the Y direction to the Z direction. In this case, the induced polarization $\boldsymbol{P}_{\mathrm{S}}^{\mathrm{R}}$ will be changed from the value given by the second pair of equations in (7) to the third pair.

The change of $\boldsymbol{P}_{\mathrm{S}}^{\mathrm{R}}$ due to domain switching will lead to a change in the intensity of the scattered light. To see this, let us consider the electric field $\boldsymbol{E}$ generated by a Fourier component $\boldsymbol{P}_{\mathrm{s}}^{K_{\mathrm{s}}} \exp(\mathrm{i}(\boldsymbol{K}_{\mathrm{s}} \cdot \boldsymbol{r} - \omega_{\mathrm{s}} t))$ of $\boldsymbol{P}_{\mathrm{S}}^{\mathrm{R}}$ with a wave vector $\boldsymbol{K}_{\mathrm{s}}$ (direction of propagation of the light). Since the electric field $\boldsymbol{E}$ has to satisfy the following Maxwell's equation:

$$\nabla \times \nabla \times \boldsymbol{E} - \varepsilon_0 \mu_0 \underline{\underline{\varepsilon}}\,\underline{\underline{\mu}}\boldsymbol{E} = \frac{\omega_{\mathrm{s}}^2}{\varepsilon_0 c^2}\underline{\underline{\mu}}\boldsymbol{P}_{\mathrm{s}}^{K_{\mathrm{s}}} \exp(\mathrm{i}\boldsymbol{K}_{\mathrm{s}} \cdot \boldsymbol{r}) \tag{8}$$

and for a non-ferrite material, $\underline{\underline{\mu}} \approx \underline{\underline{1}}$, the solution to (8) may be written as

$$\boldsymbol{E} = \boldsymbol{E}^{\mathrm{h}} + \boldsymbol{E}^{\mathrm{i}}\,, \tag{9}$$

with the homogeneous part $\boldsymbol{E}^{\mathrm{h}}$ satisfying

$$\left[\boldsymbol{k}_{\mathrm{s}} \cdot \boldsymbol{k}_{\mathrm{s}}\underline{\underline{1}} - \boldsymbol{k}_{\mathrm{s}} \otimes \boldsymbol{k}_{\mathrm{s}} - \underline{\underline{\varepsilon}}\frac{\omega_{\mathrm{s}}^2}{c^2}\right]\boldsymbol{E}^{\mathrm{h}} = 0 \tag{10}$$

and the inhomogeneous part $\boldsymbol{E}^{\mathrm{i}}$ being given by

$$\boldsymbol{E}^{\mathrm{i}} = \frac{\omega_{\mathrm{s}}^2}{\varepsilon_0 c^2}\underline{\underline{L}}^{-1}\boldsymbol{P}_{\mathrm{s}}^{K_{\mathrm{s}}} \exp(\mathrm{i}\boldsymbol{K}_{\mathrm{s}} \cdot \boldsymbol{r})\,. \tag{11}$$

Here, we denote

$$\underline{\underline{L}} \equiv \boldsymbol{K}_{\mathrm{s}} \cdot \boldsymbol{K}_{\mathrm{s}}\underline{\underline{1}} - \boldsymbol{K}_{\mathrm{s}} \otimes \boldsymbol{K}_{\mathrm{s}} - \underline{\underline{\varepsilon}}\frac{\omega_{\mathrm{s}}^2}{c^2} \tag{12}$$

and $\boldsymbol{k}_{\mathrm{s}}$ a wave vector (direction of propagation) for $\boldsymbol{E}^{\mathrm{h}}$, $\underline{\underline{\varepsilon}}$ being the relative dielectric tensor for the material.

Since $\boldsymbol{P}_{\mathrm{S}}^{\mathrm{R}}$ may be expressed as

$$\boldsymbol{P}_{\mathrm{S}}^{\mathrm{R}} = \sum_{K_{\mathrm{s}}} \boldsymbol{P}_{\mathrm{s}}^{K_{\mathrm{s}}} \exp(\mathrm{i}(\boldsymbol{K}_{\mathrm{s}} \cdot \boldsymbol{r} - \omega_{\mathrm{s}} t))\,, \tag{13}$$

the inhomogeneous part $\boldsymbol{E}_{\mathrm{i}}$ of the electric field generated by the inelastically induced polarization $\boldsymbol{P}_{\mathrm{S}}^{\mathrm{R}}$ is

$$\boldsymbol{E}_{\mathrm{i}} = \sum_{K_{\mathrm{s}}} \boldsymbol{E}^{\mathrm{i}} = \sum_{K_{\mathrm{s}}} \frac{\omega_{\mathrm{s}}^2}{\varepsilon_0 c^2}\underline{\underline{L}}^{-1}\boldsymbol{P}_{\mathrm{s}}^{K_{\mathrm{s}}} \exp(\mathrm{i}\boldsymbol{K}_{\mathrm{s}} \cdot \boldsymbol{r})\,. \tag{14}$$

For the backscattering situation such as that used in our experimental setting, the electric field associated with the backscattered light may be found by requiring continuity of the scattered light at the scattering surface, i.e.

$$\boldsymbol{E}_{\mathrm{s}} = (\boldsymbol{E}_{\mathrm{i}}|_{\boldsymbol{r}=0} \cdot \boldsymbol{e}_{\mathrm{s}})\boldsymbol{e}_{\mathrm{s}} = \left(\boldsymbol{e}_{\mathrm{s}} \cdot \sum_{K_{\mathrm{s}}} \frac{\omega_{\mathrm{s}}^2}{\varepsilon_0 c^2}\underline{\underline{L}}^{-1}\boldsymbol{P}_{\mathrm{s}}^{K_{\mathrm{s}}}\right)\boldsymbol{e}_{\mathrm{s}}\,, \tag{15}$$

where $\boldsymbol{e}_{\mathrm{s}}$ is the direction of the optical slit for the backscattered light.

For the case of a tetragonal single crystal in an experimental setting as shown in Fig. 1b, suppose that both directions of propagation of incident and backscattered light are parallel to the X-axis with the optical slits parallel to the Y-axis and that the c edge of the lattice is originally parallel to the Z-axis. Then, the polarized electric fields for this situation and for the case when the single crystal rotates 90° about the X-axis are

$$\boldsymbol{E}_{\mathrm{s}}^{1}=\left[\sum_{K_{\mathrm{s}}}\frac{\omega_{\mathrm{s}}^{2}}{\varepsilon_{0}c^{2}}\frac{\left[\boldsymbol{P}_{\mathrm{s}}^{K_{\mathrm{s}}}\right]_{2}}{\boldsymbol{K}_{\mathrm{s}}\cdot\boldsymbol{K}_{\mathrm{s}}-\varepsilon_{22}\frac{\omega_{\mathrm{s}}^{2}}{c^{2}}}\right]\boldsymbol{e}_{\mathrm{s}} \tag{16a}$$

and

$$\boldsymbol{E}_{\mathrm{s}}^{2}=\left[\sum_{K_{\mathrm{s}}}\frac{\omega_{\mathrm{s}}^{2}}{\varepsilon_{0}c^{2}}\frac{\left[\boldsymbol{P}_{\mathrm{s}}^{K_{\mathrm{s}}}\right]_{3}}{\boldsymbol{K}_{\mathrm{s}}\cdot\boldsymbol{K}_{\mathrm{s}}-\varepsilon_{33}\frac{\omega_{\mathrm{s}}^{2}}{c^{2}}}\right]\boldsymbol{e}_{\mathrm{s}} \tag{16b}$$

respectively, where $[\boldsymbol{P}_{\mathrm{s}}^{K_{\mathrm{s}}}]_2$ and $[\boldsymbol{P}_{\mathrm{s}}^{K_{\mathrm{s}}}]_3$ denote the second and third components of $\boldsymbol{P}_{\mathrm{s}}^{K_{\mathrm{s}}}$ and ε_{22} and ε_{33} the relative dielectric constants along b and c edges of the lattice, respectively. For a tetragonal crystal with a $4mm$ symmetry, $\varepsilon_{22}\neq\varepsilon_{33}$. Furthermore, (13) indicates that $[\boldsymbol{P}_{\mathrm{s}}^{K_{\mathrm{s}}}]_2$ and $[\boldsymbol{P}_{\mathrm{s}}^{K_{\mathrm{s}}}]_3$ are related to the second and the third components of $\boldsymbol{P}_{\mathrm{S}}^{\mathrm{R}}$, which are not the same, in general, according to (7).

In the above analysis, we have shown that a 90° rotation of polarization of a tetragonal single crystal about the direction of propagation of the incident and scattered light leads to a variation in the electric field for the backscattered light. For a polycrystalline material as in the present case of PLZT specimens, the measured Raman intensity should be a collection of the overall information in electric domains within the area covered by a laser beam spot ($\sim 3\ \mu\mathrm{m}$). Normally, each grain in a polycrystalline material consists of many electric domains with different orientations. Assume that in a spot covered by the laser beam, there are m lattices with different orientations. Furthermore, due to symmetry of the lattice structure, there may be n_i ($i=1,2,\ldots,m$) different electric domains in each lattice. The largest possible n_i is 6. Since $\underline{\underline{\chi}}(\boldsymbol{u})$ represents average information on the spot covered by the laser beam, it may be calculated by

$$\underline{\underline{\chi}}(\boldsymbol{u})=\frac{1}{N}\sum_{i=1}^{m}\sum_{j=1}^{n_{\mathrm{i}}}\underline{\underline{\chi}}^{ij}(\boldsymbol{u})\,, \tag{17}$$

where N in (17) is the total number of electric domains with different directions of polarization covered by the incident light; $N=n_1+n_2+\cdots+n_m$. Clearly, a 90° domain switching in the material at the spot means a change in an average orientation of electric domains, which would lead to changes in $\underline{\underline{\chi}}(\boldsymbol{u})$ and $\partial\underline{\underline{\chi}}(\boldsymbol{u})/\partial\boldsymbol{u}\big|_{\boldsymbol{u}=0}$ and, accordingly, to a change in the induced polarization $\boldsymbol{P}_{\mathrm{S}}^{\mathrm{R}}$ as indicated in (3b).

Apparently, effects of a change in $\boldsymbol{P}_{\mathrm{S}}^{\mathrm{R}}$ due to domain switching on the electric field of backscattered light are more complicated and difficult to evaluate due to the existence of grain boundaries, a non-uniform distribution of orientations of crystal lattices, etc. However, such a material has an anisotropic dielectric tensor, which is the same as that for a single tetragonal crystal. Because of this, a 90° rotation of its average polarization about the propagation direction of the incident and the scattered light is similar to that for a single tetragonal crystal. We expect a change in the intensities of the backscattered light as we observed in the experiments. Though we observed an increase in the intensity of the Raman spectrum when the average direction of polarization is rotated to be parallel to the optical slit for the backscattered light, a detailed interpretation is needed to explain the cause of this phenomenon. We will pass it here to a future analysis.

5 Summary and conclusion

Raman spectroscopy was employed to observe in-situ domain switching under an applied electric field and during a process of electric fatigue. The observation in the 90° rotation experiment verified the change in Raman intensity induced by 90° domain switching in PLZT ceramics. Using the established technique, the variations in relative intensity of the Raman spectrum with the magnitude of applied electric field or the cycle number of electric fatigue were studied and were briefly discussed. It was confirmed that the intensity of the Raman spectrum is highly dependent on the orientation of the domain switching with respect to the polarization direction of Raman incident light. A more significant decrease in relative Raman intensity was obtained for the out-of-plane poled PLZT specimens as compared with the unpoled and in-plane poled specimens. However, a complete quantitative analysis for the link between the intensity of the Raman spectrum and the domain switching in ferroelectrics at the microscopic level is still difficult and awaits a further exploration.

ACKNOWLEDGEMENTS The authors wish to acknowledge the financial support from the National Natural Science Foundation of China under Grant No. 10472098.

REFERENCES

1 E.C. Subbarao, M.C. McQuarrie, W.R. Buessem, J. Appl. Phys. **28**, 1194 (1957)
2 T. Zhu, W. Yang, Mech. Phys. Solids **47**, 81 (1999)
3 D. Wang, Y. Fotinich, G.P. Carman, J. Appl. Phys. **83**, 5342 (1998)
4 J.L. Jones, C.R.J. Salz, M. Hoffman, J. Am. Ceram. Soc. **88**, 2788 (2005)
5 M. Hammer, C. Monty, A. Endriss, M.J. Hoffmann, J. Am. Ceram. Soc. **81**, 721 (1998)
6 Y.Z. Huo, Q. Jiang, Smart Mater. Struct. **6**, 441 (1997)
7 Y. Zhang, X. Cheng, R. Qian, Mater. Sci. Eng. A **351**, 81 (2003)
8 D.C. Lupascu, *Fatigue in Ferroelectric Ceramics and Related Issues* (Springer, New York, 2004)
9 L.M. Eng, M. Abplanalp, P. Gunter, H.-J. Guntherodt, J. Phys. IV France **8**, 201 (1998)
10 L.M. Eng, Nanotechnology **10**, 405 (1999)
11 F. Wang, Y.J. Su, J.Y. He, L.J. Qiao, W.Y. Chu, Scripta Mater. **54**, 201 (2006)
12 E.K.W. Goo, R.K. Mishra, G. Thomas, J. Appl. Phys. **52**, 2940 (1981)
13 Y.H. Hu, H.M. Chan, X.W. Zhang, M.P. Harmer, J. Am. Ceram. Soc. **69**, 594 (1986)
14 T. Mallis, H. Gleiter, J. Appl. Phys. **47**, 5195 (1976)
15 X.L. Tan, Z.K. Xu, J.K. Shang, Mater. Sci. Eng. A **314**, 157 (2001)
16 X.P. Li, W.Y. Shih, J.S. Vartuli, D.L. Milius, I.A. Aksay, W.H. Shih, J. Am. Ceram. Soc. **85**, 844 (2002)
17 M. Liu, K.J. Hsia, Appl. Phys. Lett. **83**, 3978 (2003)
18 Y. Zhang, Z.W. Chen, X. Cheng, S. Zhang, Acta Metall. Sin. **40**, 1299 (2004)

19 Z.W. Chen, X. Cheng, Y. Zhang, Rare Met. Mater. Eng. **33**, 847 (2004)
20 Z.W. Chen, X. Cheng, Y. Zhang, Rare Met. Mater. Eng. **33**, 673 (2004)
21 T.G. Spiro, P. Stein, Ann. Rev. Phys. Chem. **28**, 501 (1977)
22 G. Burns, B.A. Scott, Phys. Rev. Lett. **25**, 167 (1970)
23 G. Burns, B.A. Scott, Phys. Rev. B **7**, 3088 (1973)
24 M.D. Fontana, H. Idrissi, G.E. Kugel, K. Wojcik, J. Phys. C Condens. Matter **3**, 8695 (1991)
25 A.E. Pasto, R.A. Condrate Sr., J. Am. Ceram. Soc. **56**, 436 (2002)
26 S. Pojprapai, J.L. Jones, M. Hoffman, Appl. Phys. Lett. **88**, 162 903 (2006)
27 G. Burns, B.A. Scott, Phys. Rev. Lett. **25**, 1191 (1970)
28 A.G. Souza Filho, P.T.C. Freire, J.M. Sasaki, I. Guedes, J. Mendes Filho, F.E.A. Melo, E.B. Araujo, J.A. Eiras, Solid State Commun. **112**, 383 (1999)
29 J. Rouquette, J. Haines, V. Bornand, M. Pintard, P. Papet, B. Bonnet, F.A. Gorelli, Solid State Sci. **5**, 451 (2003)
30 I. El-Harrad, C. Carabatos-Nedelec, A. Ridah, Vib. Spectrosc. **26**, 7 (2001)
31 W.H. Xu, D.X. Lu, T.Y. Zhang, Appl. Phys. Lett. **79**, 4112 (2001)
32 H.X. Zhang, A. Uusimaki, S. Leppavuori, P. Karjalainen, J. Appl. Phys. **76**, 4294 (1994)
33 S. Zhang, X. Cheng, Y. Zhang, Acta Metall. Sin. **41**, 663 (2005)